Sea Ice and Ocean Response to a Strong Mid-Winter Cyclone in the Arctic Ocean

[1]Daniel M. Watkins, [2]Ola P.G. Persson, [3]Jennifer K. Hutchings, [4]Timothy P. Stanton, [2]Amy Solomon

(1) Brown University, Providence, RI (2) Cooperative Institute for Research in Environmental Sciences and NOAA Physical Sciences Laboratory, Boulder, CO
(3) Oregon State University, Corvallis, OR (4) Moss Landing Marine Laboratories and Naval Postgraduate School, Monterey, CA

School of Engineering BROWN UNIVERSITY

INTRODUCTION Sea ice mediates the exchange of momentum, heat, and moisture between the atmosphere and the ocean. Cyclones produce strong wind gradients, imparting stress into the ice and causing deformation. In turn, increased sea ice drift speeds and rapid changes in drift direction during cyclone passage increases the momentum flux into the upper ocean. Spatial and temporal scales of mesoscale processes within a cyclone, including the development of fronts and low-level jets (LLJs) as well as the translation speed of the system, affect the stresses experienced by the ice at the surface. Motion of ice relative to the underlying ocean, in turn, results in stresses at the ice-ocean interface. In this study, we examine the sea ice and ocean response to a strong cyclone that impacted the Multidisciplinary drifting Observatory for the Study of Arctic Climate (MOSAiC) site during January and February, 2020 using an array of autonomous sensors comprising the MOSAiC Distributed Network (DN). The kinematic sea ice response to the storm shows close correspondence with the evolution of a strong LLJ. We show that the net ice movement is dependent on its position relative to the cyclone track. We discuss the spatial patterns of deformation at small and larger scales. Finally, we discuss implications for Arctic coupled model development.

DATA The MOSAiC observatory and surrounding DN were deployed in remnant first and second year ice north of the Laptev Sea at the beginning of the freeze-up season in 2019. Details of the deployment and equipment are available in a series of overview publications (Nicolaus et al. 2022, Rabe et al. 2022, Rabe et al. 2023, Schupe et al. 2022).

Central Observatory (CO)
- 4x daily radiosondes
- Meteorological tower (Cox et al., 2023)
- Autonomous Ocean Flux Buoy (AOFB, Stanton et al. 2012)

L-sites
- Autonomous Surface Flux Stations (ASFSs, Cox et al., 2023)
- AOFBs

P-sites
- 57 GPS buoys
- Network of positions allows measurement of velocity and velocity gradients

ERA5 reanalysis (Hersbach et al. 2020)
- Radiosondes and subset of P-site met observations assimilated

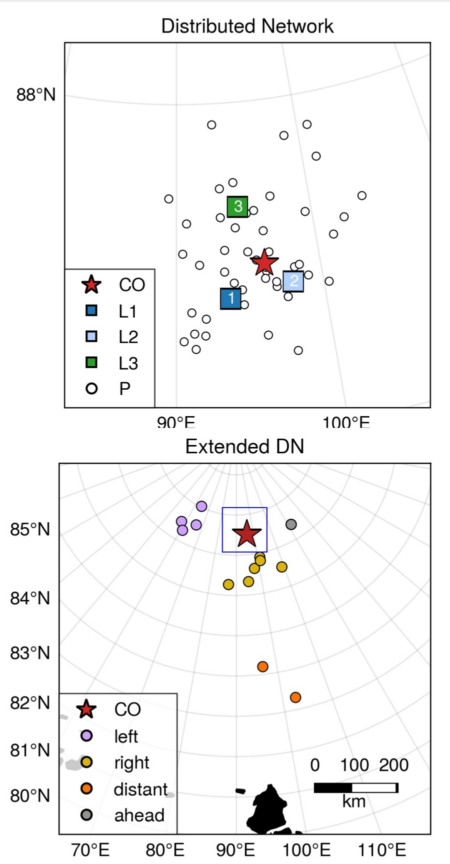

Figure 1. Positions of MOSAiC buoys and observatories on February 1st, 2020. Buoys in the ExDN are color-coded based on orientation relative to the storm track.

SYNOPTIC SETTING

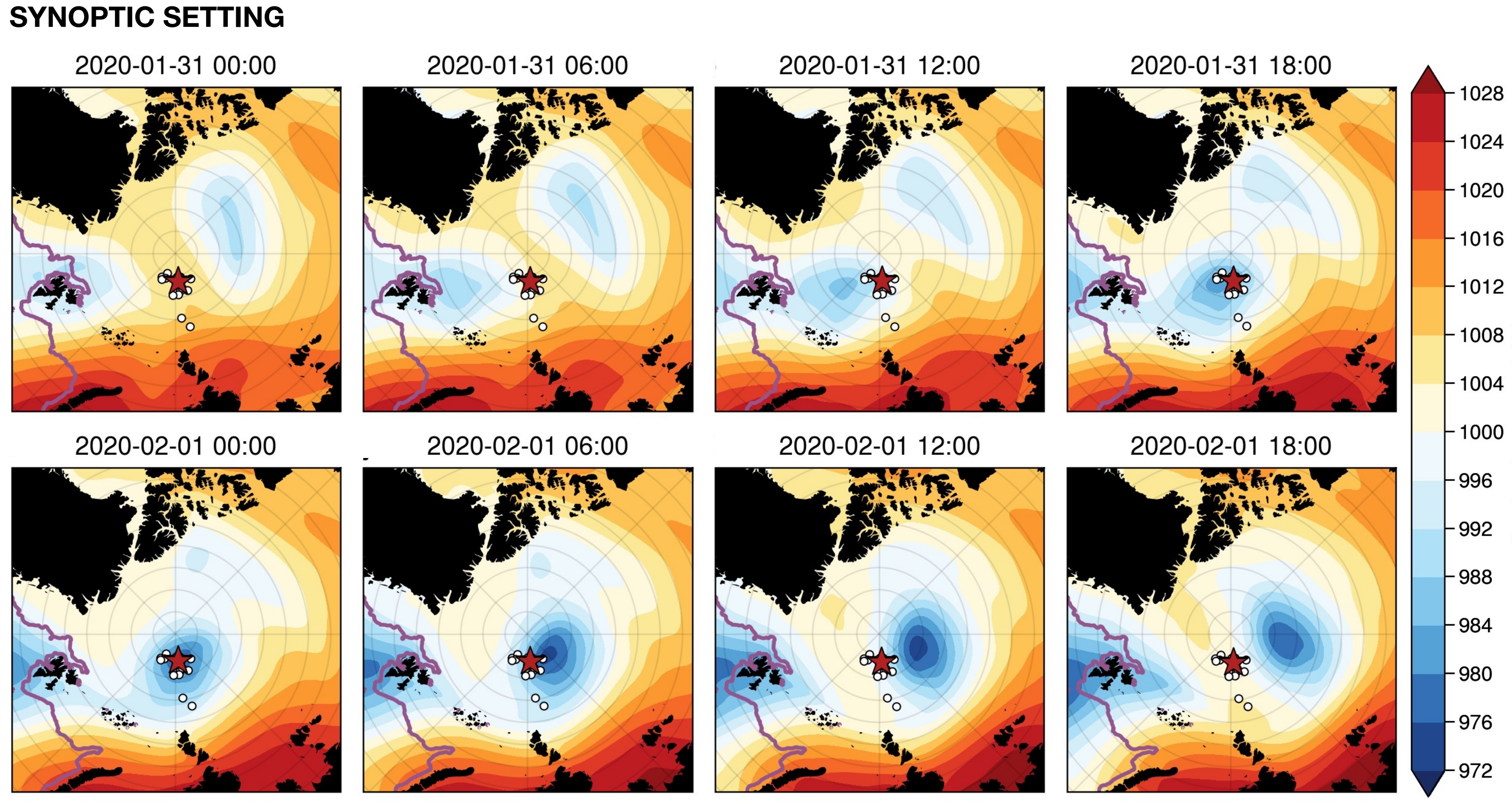

Figure 2. Mean sea level pressure from the ERA5 Reanalysis obtained via the Copernicus Data Service. The location of the CO is marked with a red star. Two cyclones crossed the MOSAiC observatory in late January and early February 2020, we focus here on the second, which can be seen forming as a depression over Svalbard on 31 January, deepening as it reaches the MOSAiC site near the North Pole.

Numerous cyclones influenced the conditions at MOSAiC observatory (Rinke et al. 2021). The 1 February cyclone was one of the strongest Arctic winter cyclones of 2019-2020. We focus on this cyclone as it produced the highest winter sea ice drift speeds and the highest drift speed variance (indicating strong deformation) observed during MOSAiC. Because coupled observations of high-Arctic cyclones in pack ice are rare, this case is an opportunity to describe the cyclone physics and ice-ocean impacts in detail for use in evaluating and improving coupled models.

CYCLONE STRUCTURE

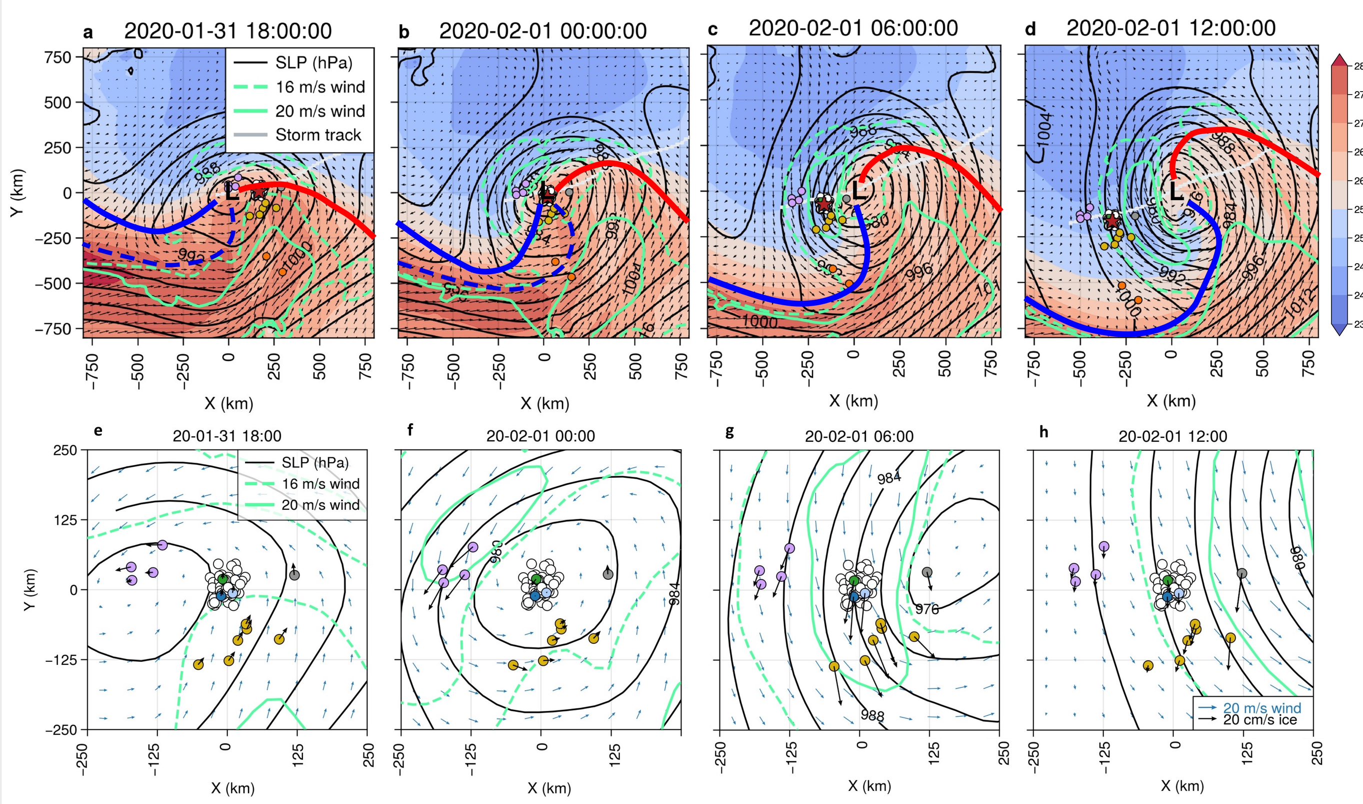

Figure 3 Panels a-d: ERA5 meteorology (shading: equivalent potential temperature; green contours: 950 hPa wind speed; arrows: 10-m wind velocity; black contours: mean sea level pressure) and MOSAiC buoy positions. Blue and red lines show the position of manually identified fronts (solid: surface; dashed: upper air). Images are centered on the position of the local ERA5 sea level pressure minimum. Panels e-h: ERA5 meteorology as above, with sea ice drift speed velocity (black arrows) for select sites in the DN and ExDN.

- The DN is initially in the warm sector, and the cold front passes over the DN from 01 to 03:00 UTC on 1 February.
- Soundings reveal the development of a low level jet (LLJ), the erosion of the near-surface Arctic inversion, and a deepening of the surface mixed layer (not shown).
- LLJ first develops in the warm sector, then behind the cold front, before finally merging to form an axisymmetric structure.
- The DN resolves spatial differences in drift speed corresponding to the location of the LLJ core (Figure 3 e-h).

SEA ICE TRAJECTORIES

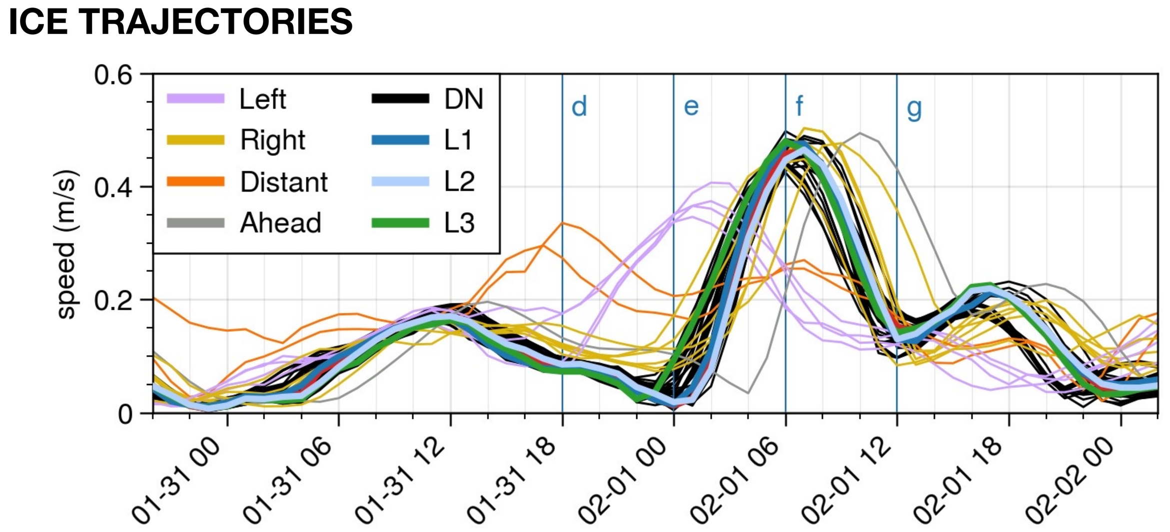

Figure 4. Sea ice drift speed. Colors as in Figure 1. Vertical lines mark the times shown in Figure 3: (d) 1/31 18Z, (e) 2/01 0Z, (f) 2/01 6Z, (g) 2/01 12Z

- Local drift speed maxima trace passage of the storm
- Secondary increase in drift speed at 16Z produced by strong inertial oscillation

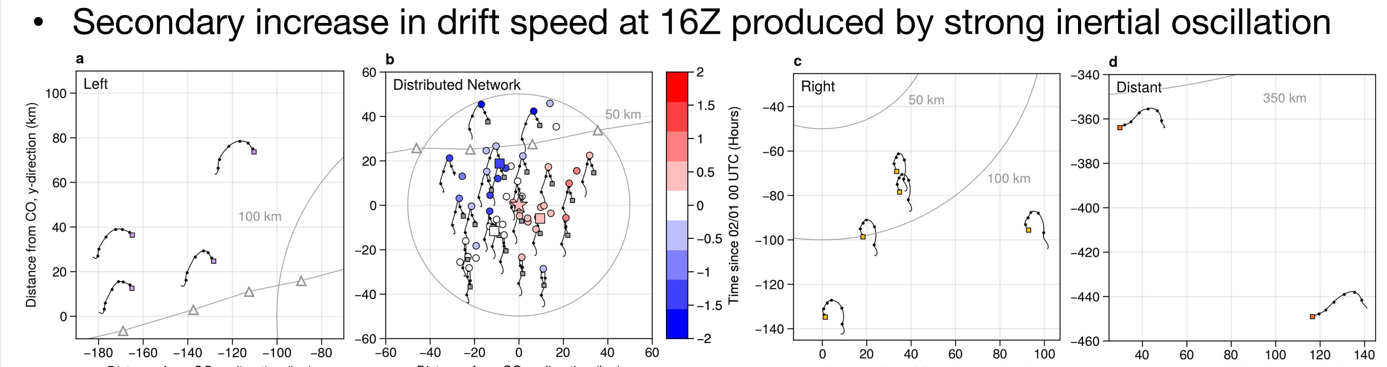

Figure 5. Trajectories of P-sites from 31 January (square) to 2 February. Dots mark 6-hour intervals. Colors in b indicate the time of the reversal in drift direction ("cusp"). Gray circles show distance from the CO. Gray triangles mark hourly positions of the storm track.

- Coherent sea ice drift response to the cyclone structure at medium to large scales (100+ km) depends on the location of the storm track.
- Sharp reversals near the storm track
- Gradual clockwise path to the right, counterclockwise to the left

SEA ICE DEFORMATION

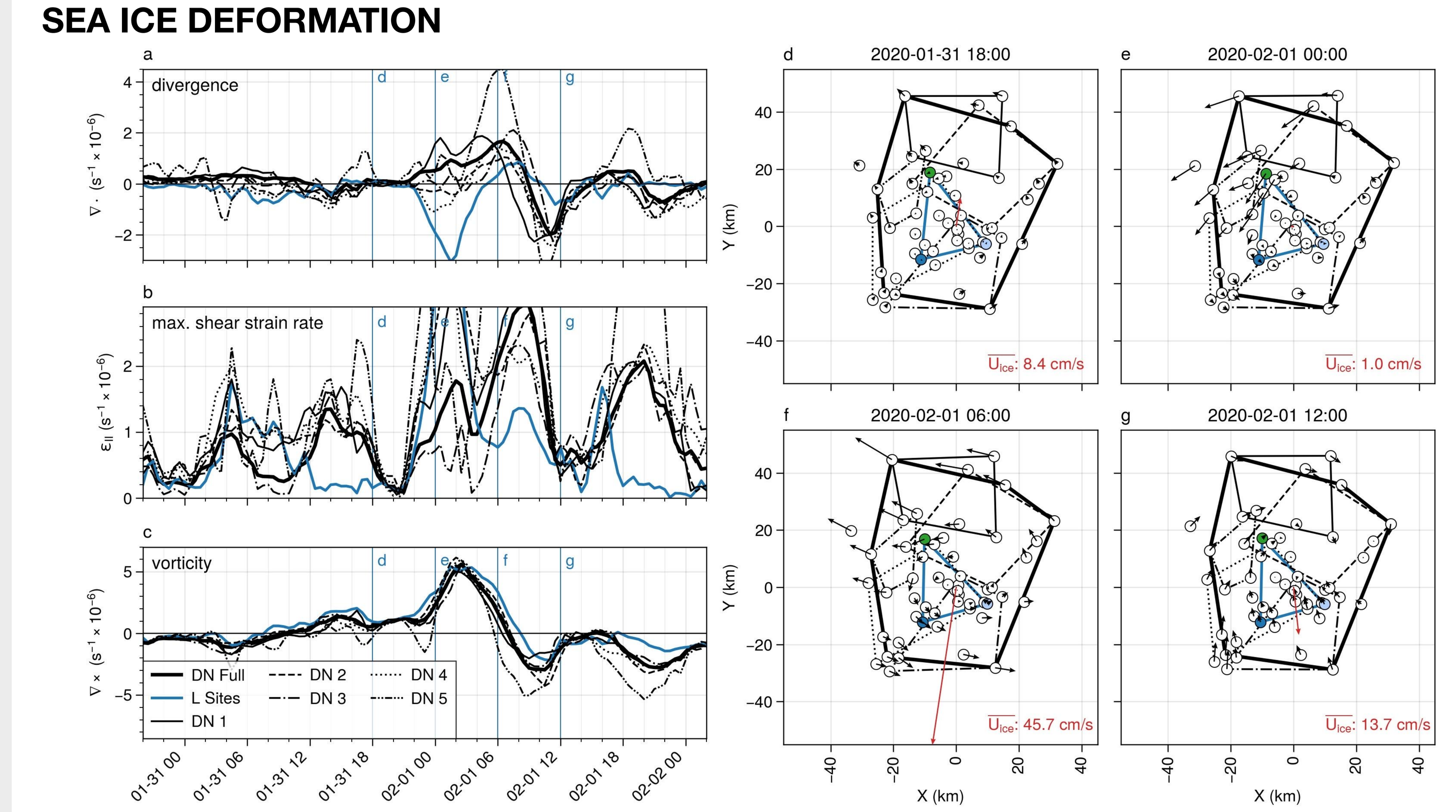

Figure 6. Area-averaged sea ice strain rate components (a-c) estimated using polygons formed by subsets of the buoy array. Panels d-g show the polygons and the drift speed anomalies (black arrows) relative to the mean DN velocity (red arrows).

- The strongest deformation response occurs as the low-level jet passes over the DN
- Divergence as the LLJ approaches, and convergence as it leaves.
- Activation of shear zones (e.g., L-site triangle in Figure 6e) causes deviation from local forcing
- Secondary local maximum in shear coincides with an inertial oscillation.

AIR-ICE-OCEAN COUPLING

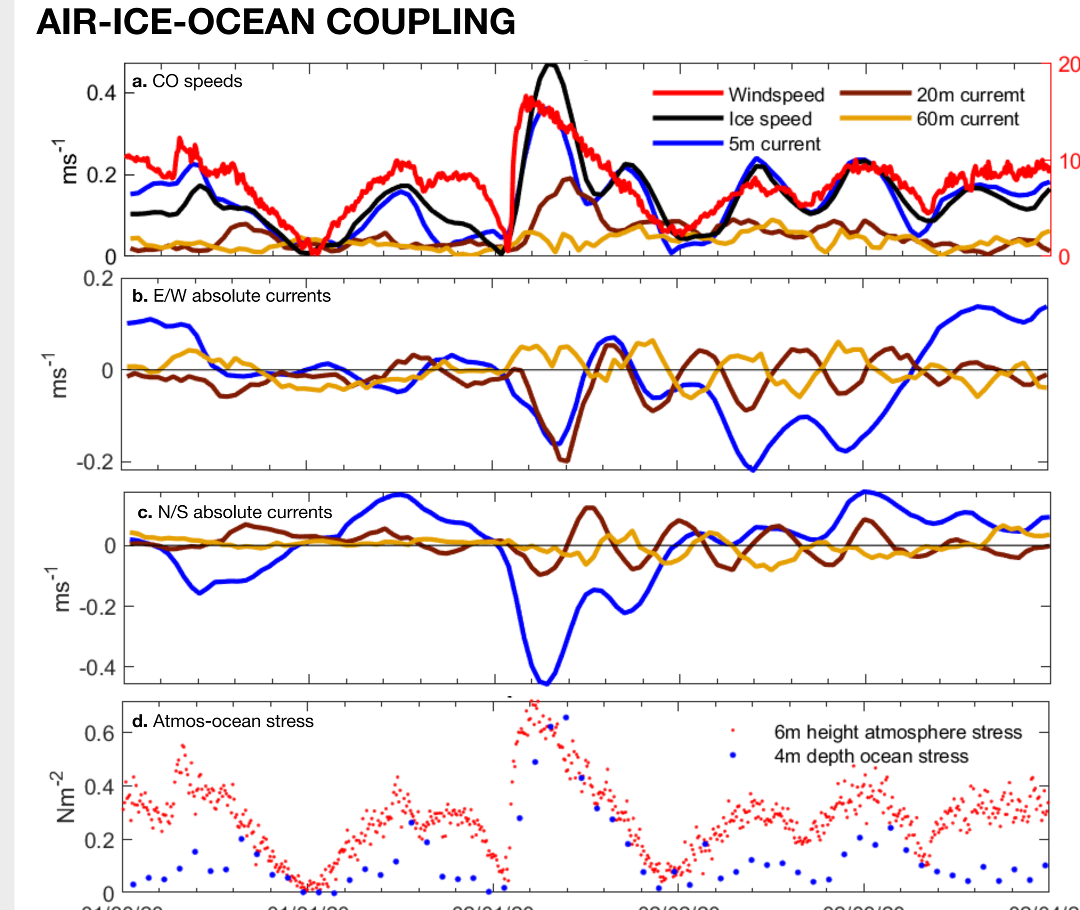

Figure 7. Ocean, ice, and atmospheric measurements at the CO. (a) Wind, ice, and ocean speeds (b) u component of ocean velocity (c) v component of ocean velocity (d) 6m atmospheric stress and 4m depth ocean stress.

- Wind speed, sea ice speed, and 5-m ocean current speed are closely coupled
- Sharp increase in wind speed on 1 February results in a jump in atmosphere stress and ocean stress, initiating inertial ringing
- Transfer of momentum downward is seen in the lag of the inertial signal with depth
- Subsurface inertial ringing continues, while surface follows changing synoptic conditions

SUMMARY We present detailed observations of coupled air-ice-ocean variability from an intense mid-winter cyclone over central Arctic pack ice. The observations show the spatial structure of air-ice-ocean interaction with unprecedented detail. We show that the development of a low-level jet is a key component for timing, scale, and intensity of the sea ice kinematic response. The horizontal structure of the cyclone wind fields produces a spatial gradient in sea ice motion, resulting in deformation of the ice pack, with a clear dependence on the stage of cyclone development and the location of the storm track. The sharp change in air-ice stresses produced by the LLJ sets off inertial ringing in the ocean, prolonging the sea ice deformation.

The results reinforce the notion that cyclone processes are a key feature of the coupled Arctic air-ice-ocean system. In particular, models with insufficient ice-ocean coupling will underestimate the deformation produced by cyclone passage. A major motivation for this work was to identify key processes for model validation. A companion study (Solomon et al., in prep) examines this event in detail using forecast runs of the Coupled Arctic Forecast System Model and the ECMWF Integrated Forecast System. Moving forward, we will examine the role of cyclone evolution and location in sea ice deformation across the full MOSAiC year.

REFERENCES

Bliss, A. C., Hutchings, J. K., & Watkins, D. M. (2023). Sea ice drift tracks from autonomous buoys in the MOSAiC Distributed Network. *Scientific Data*, 10(403), 1–10. https://doi.org/10.1038/s41597-023-02311-y
Cox, C. J., et al. (2023). Continuous observations of the surface energy budget and meteorology over the Arctic sea ice during MOSAiC. *Scientific Data*, 10(1), 519. https://doi.org/10.1038/s41597-023-02415-5
Nicolaus, M., et al. (2022). Overview of the MOSAiC expedition: Snow and sea ice. *Elementa: Science of the Anthropocene*, *10*(1). https://doi.org/10.1525/elementa.2021.000046
Hersbach, H., et al. (2020). The ERA5 global reanalysis. *Quarterly Journal of the Royal Meteorological Society*, June, 1999–2049. https://doi.org/10.1002/qj.3803
Hutchings, J. K., et al. (2011). Spatial and temporal characterization of sea-ice deformation. *Annals of Glaciology*, 52(57 PART 2), 360–368. https://doi.org/10.3189/172756411795931769
Hutchings, J. K., et al. (2018). Corrigendum: Spatial and temporal characterisation of sea-ice deformation. *Journal of Glaciology*, 64(244), 343–346. https://doi.org/10.1017/jog.2018.11
Nicolaus, M., et al. (2022). Overview of the MOSAiC expedition: Snow and sea ice. *Elementa: Science of the Anthropocene*, 10(1). https://doi.org/10.1525/elementa.2021.000046
Rabe, B., et al. (2022). Overview of the MOSAiC expedition: Physical oceanography. *Elementa: Science of the Anthropocene*, *10*, 1–31. https://doi.org/10.1525/elementa.2021.00062
Rabe, B., et al. (2023, in revision). The MOSAiC Distributed Network: observing the coupled Arctic system with multidisciplinary, coordinated, platforms. *Elementa: Science of the Anthropocene*
Rinke, A., et al. (2021). Meteorological conditions during the MOSAiC expedition. *Elementa: Science of the Anthropocene*, 9(1), 1–17. https://doi.org/10.1525/elementa.2021.00023
Shupe, M. D., et al. (2022). Overview of the MOSAiC expedition-Atmosphere. *Elementa: Science of the Anthropocene*, 10(1), 1–54. https://doi.org/10.1525/elementa.2021.00060
Solomon et al., in prep: Air-Ice-Ocean Coupling During a Strong Mid-Winter Cyclone Part 2: Coupled Dynamic Processes in Models and Model Evaluations
Stanton, T. P., Shaw, W. J., & Hutchings, J. K. (2012). Observational study of relationships between incoming radiation, open water fraction, and ocean-to-ice heat flux in the Transpolar Drift: 2002-2010. *Journal of Geophysical Research: Oceans*, 117(C7), https://doi.org/10.1029/2011JC007871
Watkins et al., in prep: Air-Ice-Ocean Coupling During a Strong Mid-Winter Cyclone Part 1: Observations

We acknowledge the combined efforts of hundreds of participants and support staff in making the MOSAiC campaign a success.